

1 Heterogeneous formation and light absorption of secondary organic
2 aerosols from acetone photochemical reactions: Remarkably
3 enhancing effects of seeds and ammonia
4
5

6 Si Zhang¹, Yining Gao¹, Xinbei Xu¹, Luyao Chen¹, Can Wu^{1,2}, Zheng Li¹, Rongjie Li¹, Binyu
7 Xiao¹, Xiaodi Liu¹, Rui Li^{1,2}, Fan Zhang^{1,2}, Gehui Wang^{1,2*}
8
9

10 ¹Key Lab of Geographic Information Science of the Ministry of Education, School of
11 Geographic Sciences, East China Normal University, Shanghai 200241, China

12 ²Institute of Eco-Chongming, 20 Cuiniao Rd., Chongming, Shanghai 202150, China
13
14
15
16

17 *Corresponding author: Prof. Gehui Wang, Email: ghwang@geo.ecnu.edu.cn

18 Tel: 86-21-54341193, Fax: 86-21-54341122
19

20 **Abstract:** Secondary organic aerosols (SOA) from highly volatile organic compounds
21 (VOCs) are currently not well represented in numerical models as their heterogeneous
22 formation mechanisms in the atmosphere remain unclear. Based on the smog chamber
23 experiments, here we investigated the yield and formation pathway of SOA from acetone
24 photochemical reactions in the presence of preexisting haze particles ((NH₄)₂SO₄, and
25 NH₄HSO₄) and mineral dusts (Na₂SO₄) under ammonia-rich conditions. Our results showed
26 that the yield of acetone-derived SOA is remarkably enhanced via multiphase reactions in
27 the presence of these preexisting seeds especially for the mineral dusts. We found that
28 aerosol acidity is a key factor controlling the formation pathways of acetone-derived SOA,
29 in which organic acids, alcohol and carbonyls produced from acetone photochemical
30 reactions dissolve into the aqueous phase of the preexisting seeds and subsequently esterify
31 and/or oligomerize into SOA that consist of larger molecules on the acidic aerosols but
32 smaller molecules on the neutral mineral aerosols. Moreover, light absorption ability of the
33 acetone-derived SOA formed on (NH₄)₂SO₄ aerosols is stronger than that formed on Na₂SO₄
34 mineral particles especially in the presence of ammonia due to a formation of N-containing
35 organics. By comparing with that from methylglyoxal (MGly), we found that the total SOA
36 from acetone in the chamber is 2.8–8.2 times that from the irreversible uptake of MGly,
37 suggesting that only considering MGly as the precursor of acetone-derived SOA will
38 probably underestimate the role of acetone in the global SOA production since acetone
39 abundantly exists in the troposphere.

40 **Keywords:** Volatile organic compounds; Photochemical oxidation; Aqueous-phase reaction;
41 Polymerization; Aerosol acidity.

42

43 **1. Introduction**

44 Secondary organic aerosols (SOA) are the major component of fine particles in the
45 atmosphere and produced from the photochemical oxidation of volatile organic compounds
46 (VOCs) (Zhang et al., 2015a; Srivastava et al., 2022; Wang et al., 2016b), which
47 significantly affects human health and global climate change (Jo et al., 2023; Chowdhury et
48 al., 2022). However, current numeric models cannot predict the evolution of atmospheric
49 SOA accurately; one of reasons is that models often only consider the partitioning process of
50 condensable oxidation products of VOCs as the major formation pathway of SOA and
51 neglect the contribution of heterogeneous reactions of highly volatile VOCs to atmospheric
52 SOA (Heald et al., 2005; Li et al., 2023).

53 A number of researchers have reported that SOA formation can be promoted
54 significantly in the presence of hydrated seeds by heterogeneous reactions (Wong et al.,
55 2015; Nguyen et al., 2014; Liu et al., 2018; Ge et al., 2017). For instance, Wong et al. (2015)
56 reported that more isoprene SOA was formed on deliquescent ammonium sulfate seeds in
57 comparison with that on the efflorescent ones. Such an enhancing effect of multiphase
58 chemistry on SOA formation has also been found by Liu et al. (2018) and Wang et al. (2022) in
59 their laboratory experiments. Their results showed that SOA multiphase formation is
60 affected by the aerosol liquid phase properties such as acidity, ionic strength and mixing
61 state, which can alter the gas-to-particle phase partitioning of VOC and change the
62 formation process of SOA (Zhang et al., 2023; Riva et al., 2019; Riva et al., 2016; Bateman
63 et al., 2014; Kampf et al., 2013; Wei et al., 2022). Amorim et al. (2020) analyzed the OH
64 reactivities of organic acids in aqueous phases with different pH, and found that all the
65 organic acids exhibited larger OH reactivities under basic conditions than those under acidic
66 conditions, indicating that aerosol acidity can influence the gas-particle partitioning and the
67 multigeneration oxidation of volatile organics in liquid phase (Wei et al., 2022; Amorim et
68 al., 2021; Amorim et al., 2020; Zhao et al., 2006; Lv et al., 2022). Moreover, a few studies
69 reported that the uptake of VOC oxidation products by inorganic aerosols can be affected by
70 a salting-in/salting-out effect (Waxman et al., 2015; Wang et al., 2016a). These results
71 suggest that heterogeneous reactions of VOCs are important sources of atmospheric SOA,

72 which are complex and affected by many factors. Currently, only a limited number of
73 volatile organics, such as glyoxal, methylglyoxal (MGly), formaldehyde and epoxydiols,
74 have been investigated by chemical transport models for their contribution to the
75 atmospheric SOA through heterogeneous reactions (Heald et al., 2005; Li et al., 2023; Fu et
76 al., 2008; Moch et al., 2020). While the role of heterogeneous reactions in SOA formation
77 from many other more volatile organics in the atmosphere is still unclear and is ignored
78 generally by model work.

79 Compared to glyoxal, MGly and formaldehyde, acetone is much more volatile, which is
80 of a Henry's law constant (K_H) being 2–4 orders of magnitude lower than the three species
81 and abundantly exists in the atmosphere from the ground surface to the upper troposphere
82 (Seinfeld and Pandis, 2006). Acetone can be directly emitted from the natural and
83 anthropogenic sources and indirectly produced from oxidation of hydrocarbons (Jacob et al.,
84 2002; Wang et al., 2023). A laboratory experiment showed that deliquesced inorganic
85 aerosols may promote SOA formation from the photochemical oxidation of acetone
86 significantly (Ge et al., 2017), but up to now the yield of SOA derived from acetone
87 photochemical reactions and the impact of inorganic aerosol physicochemical properties on
88 SOA formation from acetone have not been reported. Therefore, the formation mechanism
89 and the importance of acetone-derived SOA in the atmosphere remain unclear, where
90 acetone ubiquitously co-exists with NH_3 and preexisting aerosols. MGly is an important
91 product of acetone photochemical reactions with 14% molar yield, which can partition into
92 aqueous phase followed by oligomerization, oxidation by OH or/and reaction with NH_3 or
93 organic amine to form SOA (De Haan et al., 2019; Aiona et al., 2017; Li et al., 2021b;
94 Yasmeen et al., 2010; Zhang et al., 2022). Currently, estimation of acetone-derived SOA by
95 chemical transport models only consider its product MGly as the SOA precursor (Fu et al.,
96 2008). However, Ge et al. found that other products derived from acetone photo-oxidation
97 such as alcohols and organic acids also can dissolve into the aqueous phase and transform
98 into SOA by esterification (Ge et al., 2017), indicating that only considering the uptake of
99 MGly will probably underestimate the contribution of acetone to the global SOA production.
100 Thus, it is necessary to investigate the SOA formation from acetone and compare it with

101 MGly-SOA.

102 In this work, we quantitatively investigated the effects of deliquescent seeds and NH₃
103 on SOA formation from the photochemical reaction of acetone via chamber experiments,
104 and compared the difference of SOA formation processes in the presence of different seed
105 particles. We for the first time revealed a key role of seed acidity in controlling the yield and
106 formation pathways of SOA from acetone photochemical reactions, in which NH₃ and dust
107 particles can greatly enhance the production and light absorption of acetone-derived SOA.

108 **2. Experiments section**

109 **2.1 Materials and methods**

110 All batch mode experiments in this study were performed in a 4 m³ sealed Teflon smog
111 chamber (Figure S1). Firstly, zero air and seed particles were introduced into the chamber.
112 Then, acetone, H₂O₂ and NH₃ were introduced sequentially for the heterogeneous reactions.
113 The experiment details are reported by our previous studies (Ge et al., 2019; Zhang et al.,
114 2021; Liu et al., 2021a).

115 Briefly, zero air produced by the Zero Air Supply (Model 111 and Model 1150, Thermo
116 Scientific, USA) was used as the background gas in this study. Saturated water vapor flow
117 produced by bubbling zero air through ultrapure water (Milli Q, 18.2 MΩ, Millipore Ltd.,
118 USA) was introduced into the chamber for adjusting the relative humidity (85±1.0% RH).
119 Three types of water-solutions containing Na₂SO₄, (NH₄)₂SO₄ and NH₄HSO₄ were nebulized
120 to produce seed particles. A polydisperse mode of wetted inorganic aerosols was generated
121 from the solutions by using a single jet atomizer (7388SJA, TSI) and directly introduced into
122 the chamber as droplets without any dessication. Reactant gases including acetone, H₂O₂,
123 NH₃ and SO₂ were added separately into the chamber along with a N₂ flow using a glass
124 syringe (Liu et al., 2022; Liu et al., 2021b).

125 **2.2 Smog chamber experiments and characterization**

126 **2.2.1. Smog chamber experiments**

127 In this study, the chamber experiments can be divided into two phases: Phase I, SOA
128 formation from the photochemical oxidation and photolysis of acetone on aerosols was
129 investigated, in which the OH radicals were produced from the photolysis of H₂O₂ under 254

130 nm UV irradiating conditions; Phase II, the effect of NH₃ on SOA formation was explored
131 under dark conditions. The H₂O₂ concentrations injected into the chamber were 2.95×10¹³
132 molecules cm⁻³ in all experiments. The influence of different inorganic particles on the two
133 phases were studied. To compare the influence of different inorganic particles on the SOA
134 formation, SO₂ was added into the chamber after Phase II to produce (NH₄)₂SO₄ aerosols
135 during the Na₂SO₄ seed experiments. All the experiments were conducted under 85±1.0% RH
136 conditions and thus all the seeds in the chamber were deliquescent. At the end of each
137 experiment, aerosol in the chamber were collected on 47 mm quartz filters and stored at
138 -20 °C prior to analysis. The initial experimental conditions were displayed in Table S1.

139 **2.2.2. On-line monitoring**

140 RH and temperature inside the chamber were monitored online. The temperature in the
141 chamber was stabilized at 25±1°C by using air conditioners. Concentrations of VOCs and
142 SO₂ in the chamber were monitored by a proton transfer reaction time-of-flight mass
143 spectrometer (PTR-TOF-MS, Ionicon Analytik, Innsbruck, Austria) and a SO₂ analyzer
144 (Model 43i, Thermo scientific), respectively. Size distribution and mass concentration of
145 aerosols during the reaction process were measured by a scanning mobility particle sizer
146 (SMPS, model 3082, USA). The real-time chemical composition evolution of aerosols in the
147 chamber was measured by a high-resolution time-of-flight aerosol mass spectrometer (HR-
148 ToF-AMS, Aerodyne Research Ltd, USA), which was operated on a high sensitivity V-mode
149 with a 30 s time resolution. Prior to the experiments, ionization efficiency of the AMS was
150 calibrated by using 300 nm NH₄NO₃ particles and the value was 5.01×10⁻⁸, and the relative
151 ionization efficiency (RIE) for ammonium was 4.6. The RIE for sulfate was calibrated using
152 (NH₄)₂SO₄ particles, and the value was 0.8.

153 Particle wall loss in the chamber was corrected using a total-mass-concentration-based
154 method and the detailed descriptions were shown in Text S1 (Liu and Abbatt, 2021; Zhang et
155 al., 2024). The wall loss of NH₃ and VOCs in the chamber was also corrected (see the details
156 in Text S2 and S3) (Li et al., 2021a; Huang et al., 2018; Zhang et al., 2015b). Aerosol liquid
157 water content (ALWC) was estimated using the E-AIM thermodynamic model IV, and the
158 pH values of aerosols were calculated by Eq.1.

$$\text{pH} = -\log_{10} (\gamma_{\text{H}^+} m_{\text{H}^+}) \quad (1)$$

159 Where γ_{H^+} and m_{H^+} were the activity coefficient and molality of H^+ calculated by E-AIM
160 model, respectively.

161 **2.2.3. Off-line analysis of particles**

162 The collected samples were extracted with 15 mL of Milli-Q pure water in an ultrasonic
163 bath for 30 min, and filtered by a 0.45 μm PES syringe filter. The concentration of water-
164 soluble organic carbon (WSOC) and light absorption of the extracts were analyzed by a total
165 organic carbon analyzer (model TOC/TN-LCPH, Shimadzu Inc. Japan) and a liquid
166 waveguide capillary cell (model LWCC3000, Ocean Insight, USA) coupled with a UV/Vis
167 spectrophotometer (ocean insight) over a wavelength range of 200–900 nm, respectively.
168 Light absorption (Abs_λ) and mass absorption coefficient (MAC) of the water extracts were
169 calculated (see the details in Text S4). In addition, the collected particles were extracted with
170 pure methanol and analyzed for their chemical compositions using an ultrahigh-resolution
171 orbitrap mass spectrometer (Q-Exactive Orbitrap mass spectrometer, Thermo Scientific,
172 Germany) (Jia et al., 2023). Specifically, imidazole compounds (IMs) were determined using
173 the orbitrap-mass spectrometry, and the detailed analysis methods were reported in our
174 previous study (Liu et al., 2023).

175 **2.2.4. Observation-Based Chemical Box Model**

176 In this work, an observation-based model (OBM) incorporating the latest version 3.3.1
177 of MCM (MCM v3.3.1; available at <http://mcm.leeds.ac.uk/MCM/>) was utilized to simulate
178 the acetone photochemical reactions in the chamber. The observation levels of acetone,
179 acetaldehyde, formic acid and acetic acid, meteorological parameters (temperature and
180 relative humidity) and the initial H_2O_2 concentration were input into the OBM-MCM model
181 as constraints.

182 **3. Results and discussion**

183 **3.1. Formation of acetone-derived SOA**

184 Figure 1 shows the time evolution of gas and particle phase species during the reaction
185 in the presence of $(\text{NH}_4)_2\text{SO}_4$ seeds. In this study the whole smog chamber reaction process
186 consists of two phases, of which Phase I is a photochemical reaction of acetone without

187 $\text{NH}_3(\text{g})$ and Phase II is a dark reaction with introduced NH_3 . During the Phase I, once the
188 light was turned on the gas phase concentrations of MGly, acetaldehyde, formic acid and
189 acetic acid quickly increased with a decreasing acetone (Phase I, Figure 1a), while SOA
190 were instantly produced and sharply increased to over $90 \mu\text{g m}^{-3}$ (Phase I, Figure 1b). When
191 the concentration of SOA during the Phase I did not change and even started to decrease, the
192 light was turned off and $\text{NH}_3(\text{g})$ was introduced into the chamber (Phase II). According to
193 the formation time of these gas products, acetaldehyde and MGly are often taken as the first-
194 generation products, while formic and acetic acids are usually considered as the final-
195 generation products (Poulain et al., 2010). Oxidation state of compounds (OSc) and O/C
196 elemental ratio of SOA in the aerosol phase continuously increased during the reaction
197 process (Figure 1c), which is corresponding to a decreasing fraction of CHO^+ plus $\text{C}_2\text{H}_3\text{O}^+$
198 and an increasing fraction of CO_2^+ (Figure 1d), indicating an efficient conversion of
199 carbonyl compounds to carboxylic acid compounds. In the Phase I, we observed an aerosol-
200 phase decreasing trend of molar ratio of NH_4^+ to SO_4^{2-} , which was accompanied by an
201 increasing trend of N/C ratio of SOA (Figures 1b and 1c), indicating a transformation of
202 inorganic NH_4^+ to N-containing organic compounds. Such a phenomenon can be ascribed to
203 a reaction of carbonyl compounds with the $(\text{NH}_4)_2\text{SO}_4$ seeds during the Phase I (Liu et al.,
204 2023; Li et al., 2021b).

205 As shown in Figures 1a and 1b, after NH_3 was introduced (Phase II) the formic and
206 acetic acids decreased dramatically while SOA did not change obviously, suggesting that the
207 decreases of the gas acids were mainly resulted from the enhanced wall loss due to the
208 neutralization of NH_3 on the chamber wall. Interestingly, we found that during the dark
209 reaction OSc and O/C ratio of SOA decreased slightly but their N/C ratio increased
210 significantly by a factor of approximately two (Figure 1c), implying that chemical
211 composition of SOA changed remarkably after NH_3 was introduced, although the SOA mass
212 did not change evidently (Figure 1c, Phase II). Moreover, such a slight decrement of O/C
213 and a significant increment of N/C in the elemental compositions of SOA (Figure 1c) were
214 also accompanied by a sharp increase of CHN family fragment fractions (Figure 1d, Phase
215 II), which can be explained by a carbonyl-ammonium condensation under the dark

216 conditions that forms a C-N bond and loses a H₂O molecule (Aiona et al., 2017; Li et al.,
217 2021b; Liu et al., 2023). Such an aqueous-phase dark reaction after NH₃ was introduced can
218 be further revealed by a change in SOA composition during the Phase II, which is
219 characterized by higher fractions of C_xH_yN₁ fragments in the Phase II than those in the
220 Phase I (Figure 2). Organic ammonium salt would contribute NH_x fragments instead of
221 fragments containing N, C, and O elements. Therefore, the CHN species should generated
222 from the reactions of carbonyls with NH₃ rather than the acid-base neutralization of organic
223 acid with NH₃ (Liu et al., 2015). As seen in Figure S2, the CHN family species mainly
224 include CHN, CH₄N, C₂H₆N, C₂H₇N, C₂H₄N, CH₅N and C₃H₆N ions, which are similar to
225 the fragments of N-containing organics produced from the reaction of carbonyls with
226 (NH₄)₂SO₄ (De Haan et al., 2010), and increased significantly during the Phase II, resulting
227 in an enhancing role of NH₃ on the SOA formation from acetone photochemical reaction.

228 **3.2. Enhancing effect of seeds on the SOA formation**

229 As shown in Figure S3, the concentration of SOA derived from acetone photochemical
230 reactions in the presence of (NH₄)₂SO₄ seeds is twenty times higher than that in the absence
231 of the seeds, suggesting that the occurrence of (NH₄)₂SO₄ seeds remarkably promoted the
232 SOA formation. Such an enhancing role was also found for Na₂SO₄ and NH₄HSO₄ seeds
233 (Figure S4). Because of the significant influence of surface area of aerosols on the
234 multiphase reactions (Huang et al., 2016), the SOA formation amounts were normalized by
235 the aerosol surface area (SA) to eliminate the interference of the difference in seed
236 concentrations. As seen in Figure 3a, the normalized concentration of SOA on Na₂SO₄ seeds
237 is two times larger than that on (NH₄)₂SO₄ and NH₄HSO₄ seeds, respectively, indicating that
238 the difference in physicochemical properties of seeds are of different promoting effects on
239 the SOA formation. MGly is one of the first-generation oxidation products of the acetone
240 photochemical reactions and also one of the critical precursor of SOA (Li et al., 2021b).
241 Therefore, we choose it as the target compound to explore the effect of the seeds on the SOA
242 formation. The multiphase reactions of acetone-derived MGly in the chamber can be divided
243 into two processes: the gas-particle partitioning and the subsequent aqueous phase reactions
244 (Srivastava et al., 2022; Waxman et al., 2015), which are further discussed as follows:

245 **3.2.1. The effects on the gas-to-particle phase partitioning**

246 It has been reported that the presence of salts in aerosol aqueous phase can significantly
247 influence the gas-particle phase partitioning of MGly, which can decrease the solubility of
248 MGly, i.e., salting out effect (Waxman et al., 2015). In this study, the effective Henry's law
249 constants ($K_{H, \text{salt}}$) of MGly in the aqueous phase of various seeds were further estimated by
250 Eq.2 (Waxman et al., 2015; Cui et al., 2021).

$$\log \left(\frac{K_{H,w}}{K_{H,salt}} \right) = K_S c_{salt} \quad (2)$$

251 Where $K_{H,w}$ and $K_{H, \text{salt}}$ are the Henry's law constants of MGly in pure water ($3.71 \times 10^3 \text{ M}$
252 atm^{-1}) (Curry et al., 2018) and in a salt solution, respectively; K_S is the salting constant or
253 Setschenow constant, which is 0.16 M^{-1} used in this work (Waxman et al., 2015), supposing
254 that the K_S values are similar in the three types of inorganic aerosols (Gen et al., 2018); c_{salt}
255 is the salt concentration in molality.

256 As shown in Figure 3b, $K_{H, \text{salt}}$ of MGly on Na_2SO_4 seeds in this study is more than two
257 times that on $(\text{NH}_4)_2\text{SO}_4$ and NH_4HSO_4 seeds, respectively, because of its lower salt
258 concentration and weaker salting out effect. The acidity of aerosol aqueous phase also can
259 affect the uptake of MGly. For instance, Zhao et al. (2006) found that the effective Henry's
260 law constant of MGly decreased with an increase of aqueous acidity in their laboratory
261 experiments. As shown in Figure 3b, the pH values of Na_2SO_4 , $(\text{NH}_4)_2\text{SO}_4$ and NH_4HSO_4
262 seeds in our chamber study are 7.0, 4.9 and -0.2, respectively, indicating that the neutral
263 nature of Na_2SO_4 seeds is more favorable for the uptake of MGly compared to the two other
264 acidic seeds. In addition, the higher OSc and larger fraction of $\text{C}_x\text{H}_y\text{O}_z$ signals of SOA on
265 Na_2SO_4 seeds (Figure 3a and Figure S5) may also be caused by enhanced uptake of
266 carboxylic acids (e.g., formic and acetic acids) in comparison with those by other two kinds
267 of acidic seeds (Huang et al., 2016), which also resulted in the less abundant formic and
268 acetic acids in the gas phase at the end of Phase I during the Na_2SO_4 seed experiment
269 (Figure S6).

270 **3.2.2. The effects on the aqueous reaction**

271 The aqueous formation of SOA could be affected by the phase state and acidity of

272 aerosols (Amorim et al., 2020; Amorim et al., 2021; Shen et al., 2022). Since particles in all
273 the experiments of this work are deliquesced under 85% RH conditions (Wong et al., 2015;
274 Bateman et al., 2015), the influence of phase state can be neglected. Here, we focus on the
275 impact of aerosol acidity on the SOA formation pathway by characterizing the chemical
276 composition of SOA in the chamber using ESI-Q-MS technique. The mass spectra of SOA
277 formed on different seeds are shown in Figures 3c and 3d, and the detail peak assignments
278 are presented in Table S2, respectively. As shown by Figures 3c and 3d, the main peaks of
279 SOA formed on Na₂SO₄ seeds locate in the mass range lower than $m/z=200$, whereas the
280 main peaks of SOA formed on (NH₄)₂SO₄ seeds locate in the mass range larger than
281 $m/z=200$, clearly showing that SOA formed on neutral aerosols are dominated smaller
282 molecules while those formed on acidic aerosols are dominated larger molecules. The
283 phenomenon can be attributed to the promotion of the acid-catalyzed reactions in the
284 formation of high-order oligomers on the acidic seeds (Jang et al., 2002; Zhang et al.,
285 2015a). On the other hand, such different formation pathways of SOA also can be explained
286 by the difference of reactive oxygen species formed in the aqueous phase of the different
287 aerosols. On neutral aerosols, organic hydroperoxides produced from the reaction of
288 peroxides radicals and HO₂ radicals decompose and generate OH radicals through the
289 cleavage of the weaker O-O bond (Wei et al., 2022). Then, the OH radicals oxidize the
290 oligomers to low molecular weight (LMW) compounds (Zhao et al., 2017). In contrast, on
291 acidic aerosols the acid-catalyzed thermal decomposition of the organic hydroperoxides
292 leads to the formation of alcohol and ketone as the end products, which does not involve
293 radical formation (Wei et al., 2022; Yaremenko et al., 2016). Then, the carbonyls in the
294 aqueous phase will undergo hydration, oligomerization and acid-catalyzed aldol
295 condensation to form high molecular weight (HMW) compounds (Zhang et al., 2015a;
296 Kenseth et al., 2023; Li et al., 2021b). Such an explanation can be supported by the higher
297 OSc of SOA formed on the neutral aerosols (Figure 3a). On the other hand, the lower SOA
298 mass formed on acidic aerosols can also in part be attributed to the different reactivity of OH
299 radical to carboxylic group; OH radical does not react with the carboxyl group (COOH)
300 rapidly through H-abstraction from an O-H bond, but OH radical is more reactive to the

301 carboxylate group (ROO^-) by abstracting an electron, which can result in a high SOA yield
302 on neutral aerosols (Amorim et al., 2021; Herrmann et al., 2015).

303 **3.3 The different effect of NH_3 on SOA formation on different seeds**

304 As shown in Figure 4a, when NH_3 was introduced into the reaction system (Phase II),
305 the ratio of N/C of SOA increased significantly because of the reaction of $\text{NH}_4^+/\text{NH}_3$ with
306 carbonyls on acidic $(\text{NH}_4)_2\text{SO}_4$ and NH_4HSO_4 seeds, but such an evident change was not
307 observed in the presence of NH_3 for neutral Na_2SO_4 seeds. One of the reasons is that NH_3
308 dissolve more readily on acidic aerosols. The gas-to-particle phase partition coefficients of
309 NH_3 ($\epsilon(\text{NH}_4^+)$) on different seeds were calculated (Text S5) (Guo et al., 2017; Lv et al.,
310 2023). As shown in Figure 4b, $\epsilon(\text{NH}_4^+)$ is zero and 1.0 for Na_2SO_4 and NH_4HSO_4 seeds,
311 respectively, suggesting that NH_3 was almost not absorbed by Na_2SO_4 seeds but efficiently
312 absorbed by NH_4HSO_4 seeds. The phenomenon can be confirmed by the Figure S7, more N
313 mass partitioned on more acidic aerosols. Liu et al. (2015) analyzed the uptake of NH_3 onto
314 SOA and also found that the uptake coefficient positively correlated with particle acidity.
315 Several studies put forward that the reaction of NH_3 with carbonyl are likely acid-catalyzed
316 (Zhang et al., 2015a; Liu et al., 2015). However, such a conclusion was inconsistent with the
317 phenomenon observed by Yang et al. (2024); they found that the light absorption ability of
318 brown carbon produced from the aqueous reactions of α -dicarbonyls with ammonium or
319 amine increased exponentially with the increase of pH. To resolve such a disagreement. We
320 analyzed the chemical composition of SOA detected by HR-ToF-AMS at different reaction
321 phases. As shown in Figure S5a-d, no change was observed on Na_2SO_4 particles at Phase II
322 after NH_3 was introduced, but the fraction of the CHN family species increased dramatically
323 on $(\text{NH}_4)_2\text{SO}_4$ and NH_4HSO_4 particles at phase II. Hence, we supposed that NH_3 can
324 promote the formation of N-containing SOA on acidic aerosols significantly via reacting
325 with carbonyl compounds. To verify such an assumption, we performed additional
326 experiments by introducing 500 ppb SO_2 into the chamber in the presence of Na_2SO_4 seeds
327 after Phase II (Phase III, Figure S8). The addition of SO_2 resulted in $(\text{NH}_4)_2\text{SO}_4$ produced
328 immediately in the chamber (Phase III, Figure S8a), and then the fraction of CHN species
329 increased sharply (Phase III, Figure S8b). Such results again demonstrate the pivotal role of

330 acidic particles in the formation of N-containing SOA.

331 The optical properties of the acetone-derived SOA on different particles were measured
332 by LWCC. Compared with the light absorption spectra of SOA formed on Na_2SO_4 seeds in
333 the absence of SO_2 , an enhanced MAC peak at ~ 270 nm was observed for SOA formed on
334 $(\text{NH}_4)_2\text{SO}_4$ seeds and on Na_2SO_4 seeds with SO_2 , respectively (Figure 4c). Such enhanced
335 absorptions are in agreement with that of the products from MGly and $(\text{NH}_4)_2\text{SO}_4$ reaction,
336 which displays prominent peaks at <240 and ~ 270 nm with a tail extending to >350 nm
337 (Kasthuriarachchi et al., 2020). The increased absorption peak at 270 nm can be ascribed to
338 a formation of imidazoles through the reaction of MGly with NH_4^+ (You et al., 2020). In this
339 work, 1H-imidazole-4-carboxylic acid was observed for the SOA formed on $(\text{NH}_4)_2\text{SO}_4$
340 seeds (Figure 4d). However, there was no absorption peak at ~ 270 nm for the products of the
341 Na_2SO_4 particles in the absence of SO_2 (Figure 4c), further confirming the enhancement
342 effect of acidic particles on the formation of light-absorbing SOA, which is often termed as
343 brown carbon.

344 **3.4. Formation mechanisms of acetone-derived SOA on different seeds**

345 Figure 5 shows the mass yield and MAC of acetone-derived SOA at the end of Phase II.
346 Clearly, SOA is formed more readily on neutral Na_2SO_4 seeds than on acidic $(\text{NH}_4)_2\text{SO}_4$
347 seeds. However, in the presence of NH_3 , SOA formed on $(\text{NH}_4)_2\text{SO}_4$ seeds are more light-
348 absorbing than those formed on Na_2SO_4 aerosols, suggesting that a stronger acidity of
349 aerosol phase is favorable for the formation of light-absorbing organics, because NH_3 cannot
350 be taken up by neutral aerosols and thus carbonyl-ammonium condensation is only active
351 under acidic conditions and produce light-absorbing N-containing organics.

352 By combining the gas and aerosol phase chemistry evolution in the chamber, chemical
353 mechanism for SOA formation from acetone multiphase photochemical reactions on
354 different aerosols in the presence of NH_3 was proposed (Figure 6). The photochemical
355 reactions of acetone in this work include photolysis and oxidation by OH radicals, which
356 produce various peroxy radical (RO_2) and undergo two RO_2 fates, RO_2+HO_2 and RO_2+RO_2
357 reactions. The loss rates of two RO_2 pathways are shown in Figure S10. Obviously,
358 RO_2+HO_2 was the main pathway in RO_2 chemistry, the loss rate of which was 3.19 times

359 that of RO₂+RO₂ pathway. Concentrations of main gaseous products from RO₂ chemistry
360 are shown in Table S3. C₂H₄O₃ and C₃H₆O₃ are intermediate volatility organic compounds
361 (IVOCs) and can undergo gas-particle partitioning readily to form SOA. Moreover, there are
362 abundant gas-phase intermediate products containing hydrophilic functional groups such as
363 alcohol, ketone and organic acids formed from acetone photochemical reactions, which can
364 dissolve into aqueous phase and undergo further oxidation reaction, esterification reaction
365 and radical-radical reaction to form SOA on particles (Poulain et al., 2010; Ge et al., 2017).
366 For example, the dissolved MGly can be hydrolyzed and then oxidized into organic acids
367 such as pyruvic and oxalic acids or proceeds to a series of oligomerizations to produce many
368 oligomers, giving rise to SOA formation. The acetone alcohol can react with acetic acid to
369 form esters C₅H₈O₃ in aqueous phase. The organic hydroperoxide C₃H₆O₃ produced from
370 acetone-RO₂+HO₂ pathway also can react with acetic acid and pyruvic acid to form C₅H₈O₄
371 and C₆H₈O₅ in particle phase, respectively. These esterification reactions can also contribute
372 to SOA formation effectively.

373 In the presence of NH₄⁺, carbonyl compounds in the aerosol phase can react with free
374 NH₃ molecules and produce N-containing SOA including imine, imidazole and other
375 oligomers (Liu et al., 2023). LMW SOA are formed readily in neutral aerosol phase, while
376 HMW SOA and N-containing brown carbon are formed favorably in acidic aerosol phase,
377 because the acidic condition is favorable for the uptake of NH₃. The carbenium cations,
378 which are produced from protonation and dehydration of the hydration products of MGly
379 under acidic conditions, are the key intermediates for formation and propagation of
380 oligomerization (Ji et al., 2020). The oligomers and N-heterocycles are produced from the
381 nucleophilic addition of the negative hydroxyl O-atom of hydration products and the
382 negative N-atom of NH₃ to the carbenium cations, respectively (Li et al., 2021b; Li et al.,
383 2021a).

384 **3.5. Comparison of SOA from acetone with that from MGly in the chamber**

385 Currently, estimations of acetone-derived SOA by models only consider its product
386 MGly as the precursor (Fu et al., 2008). The uptake coefficient (γ) of MGly used in their
387 work is 2.9×10^{-3} without taking into account the influence of salting effects. Curry et al.

388 (2018) revised the γ to 10^{-10} - 10^{-6} after considering salting effects, aerosol thermodynamics,
 389 mass transfer, and irreversible reactions of organic species with OH in aqueous phase. In
 390 addition, previous laboratory studies showed a large difference among the uptake
 391 coefficients of MGly, ranging from 4.0×10^{-7} to 2.4×10^{-2} (Li et al., 2023; Li et al., 2021b).
 392 Salting effects and other VOCs such as formaldehyde and acetaldehyde also can influence
 393 the SOA formation from aqueous reaction of MGly (Rodriguez et al., 2017; Waxman et al.,
 394 2015). These documented values suggest a big uncertainty for SOA model work on MGly.
 395 Currently, the uptake coefficient (γ) of MGly is set as 2.6×10^{-4} in CMAQ v5.3 (Chen et al.,
 396 2021). Hence, the concentration of SOA formed in the chamber only from the irreversible
 397 uptake of MGly can be calculated by Eq.3 (Chen et al., 2021; Li et al., 2023).

$$\frac{\partial aqSOA}{\partial t} = \left(\frac{a}{D_g} + \frac{4}{v_{MGLY}\gamma_{MGLY}} \right)^{-1} A[MGLY] \quad (3)$$

398 Where $\frac{\partial aqSOA}{\partial t}$ is the formation rate of SOA in experiments; a is the effective radius of
 399 aerosols; D_g is the gas-phase molecular diffusion coefficient; V_{MGLY} is the gas-phase mean
 400 molecular speed of MGly; A is the aerosol surface area per unit air volume; $[MGly]$ is the
 401 vapor-wall loss corrected concentration of MGly (see the details in Text S3).

402 As shown in Table 1, the concentrations of the total SOA-derived from acetone
 403 photochemical reaction in the chamber is 2.8-8.2 times that only from the irreversible uptake
 404 of MGly, suggesting that only considering the role of MGly will inevitably underestimate
 405 the contribution of acetone to SOA production in the atmosphere especially in polluted
 406 urban regions, which are often characteristic of high loadings of acetone and aerosols.

407 **4. Conclusions**

408 In this study we investigated the mass yield and formation mechanism of SOA from
 409 acetone photochemical reaction in the presence of preexisting haze particles ($(NH_4)_2SO_4$ and
 410 NH_4HSO_4) and mineral dusts (Na_2SO_4) under ammonia-rich conditions. We found that the
 411 presence of seeds can significantly promote the formation of acetone-derived SOA, and the
 412 SOA yield on Na_2SO_4 seeds is larger than that on acidic $(NH_4)_2SO_4$ and NH_4HSO_4 seeds,
 413 indicating that the differences in physicochemical properties of pre-existing aerosols are of

414 different promoting effects on the acetone-derived SOA formation. In comparison with those
415 of $(\text{NH}_4)_2\text{SO}_4$, and NH_4HSO_4 seeds, the weaker salting-out effect and lower acidity of
416 Na_2SO_4 seeds are in favor of the gas-to-particle partitioning of the SOA precursors.
417 Moreover, SOA formed on the neutral seeds are dominated by smaller molecules with a
418 higher OSc, while those formed on the acidic seeds are dominated by larger molecules with
419 a lower OSc.

420 Because NH_3 cannot be taken up by neutral aerosols, heterogeneous reaction of
421 carbonyl with ammonium is only active under acidic conditions, which produces light-
422 absorbing N-containing compounds such as imidazoles, resulting in the acetone-derived
423 SOA formed on $(\text{NH}_4)_2\text{SO}_4$ seeds more light absorbing than those formed on Na_2SO_4 seeds.
424 In the chamber the total SOA-derived from acetone photochemical reaction is 2.8-8.2 times
425 that only from the irreversible uptake of MGly, suggesting that only considering the
426 irreversible uptake of MGly will inevitably underestimate the contribution of acetone
427 photochemical reactions to SOA in the atmosphere.

428

429 **ASSOCIATED CONTENT**

430 **Supplement.** The supplement related to this article is available online at: <https://doi.org/XX>.

431 **Author contribution.** SZ and GW designed the experiment. SZ, XX, and LC conducted the
432 experiments. SZ, YG, XX, LC, and GW performed the data interpretation. SZ and GW
433 wrote the paper. CW, RL, FZ, ZL, and RL contributed to the paper with useful scientific
434 discussions or comments.

435 **Competing interests.** The authors declare no competing financial interest.

436 **Disclaimer.**

437 **Acknowledgements.**

438 This work was funded by the National Natural Science Foundation of China (No.
439 42130704, U23A2030).

440 **References:**

441 Aiona, P. K., Lee, H. J., Leslie, R., Lin, P., Laskin, A., Laskin, J., and Nizkorodov, S. A.: Photochemistry of
442 products of the aqueous reaction of methylglyoxal with ammonium sulfate, ACS Earth Space Chem., 1, 522-

443 532, 10.1021/acsearthspacechem.7b00075, 2017.

444 Amorim, J. V., Guo, X., Gautam, T., Fang, R., Fotang, C., Williams, F. J., and Zhao, R.: Photo-oxidation of pinic
445 acid in the aqueous phase: a mechanistic investigation under acidic and basic pH conditions, *Environ. Sci.*
446 *Atmos.*, 1, 276-287, 10.1039/d1ea00031d, 2021.

447 Amorim, J. V., Wu, S., Klimchuk, K., Lau, C., Williams, F. J., Huang, Y., and Zhao, R.: pH dependence of the
448 OH reactivity of organic acids in the aqueous phase, *Environ. Sci. Technol.*, 54, 12484-12492,
449 10.1021/acs.est.0c03331, 2020.

450 Bateman, A. P., Bertram, A. K., and Martin, S. T.: Hygroscopic influence on the semisolid-to-liquid transition of
451 secondary organic materials, *J. Phys. Chem. A*, 119, 4386-4395, 10.1021/jp508521c, 2014.

452 Bateman, A. P., Gong, Z., Liu, P., Sato, B., Cirino, G., Zhang, Y., Artaxo, P., Bertram, A. K., Manzi, A. O., Rizzo,
453 L. V., Souza, R. A. F., Zaveri, R. A., and Martin, S. T.: Sub-micrometre particulate matter is primarily in liquid
454 form over Amazon rainforest, *Nature Geosci.*, 9, 34-37, 10.1038/ngeo2599, 2015.

455 Chen, X. Y., Zhang, Y., Zhao, J., Liu, Y. M., Shen, C., Wu, L. Q., Wang, X. M., Fan, Q., Zhou, S. Z., and Hang,
456 J.: Regional modeling of secondary organic aerosol formation over eastern China: The impact of uptake
457 coefficients of dicarbonyls and semivolatile process of primary organic aerosol, *Sci. Total Environ.*, 793,
458 148176, 10.1016/j.scitotenv.2021.148176, 2021.

459 Chowdhury, S., Pozzer, A., Haines, A., Klingmüller, K., Münzel, T., Paasonen, P., Sharma, A., Venkataraman, C.,
460 and Lelieveld, J.: Global health burden of ambient PM_{2.5} and the contribution of anthropogenic black carbon
461 and organic aerosols, *Environ. Int.*, 159, 107020, 10.1016/j.envint.2021.107020, 2022.

462 Cui, J. n., Sun, M., Wang, L., Guo, J., Xie, G., Zhang, J., and Zhang, R.: Gas-particle partitioning of carbonyls
463 and its influencing factors in the urban atmosphere of Zhengzhou, China, *Sci. Total Environ.*, 751, 142027,
464 10.1016/j.scitotenv.2020.142027, 2021.

465 Curry, L. A., Tsui, W. G., and McNeill, V. F.: Technical note: Updated parameterization of the reactive uptake of
466 glyoxal and methylglyoxal by atmospheric aerosols and cloud droplets, *Atmos. Chem. Phys.*, 18, 9823-9830,
467 10.5194/acp-18-9823-2018, 2018.

468 De Haan, D. O., Hawkins, L. N., Kononenko, J. A., Turley, J. J., Corrigan, A. L., Tolbert, M. A., and Jimenez, J.
469 L.: Formation of nitrogen-containing oligomers by methylglyoxal and amines in simulated evaporating cloud
470 droplets, *Environ. Sci. Technol.*, 45, 984-991, 10.1021/es102933x, 2010.

471 De Haan, D. O., Pajunoja, A., Hawkins, L. N., Welsh, H. G., Jimenez, N. G., De Loera, A., Zauscher, M., Andretta,
472 A. D., Joyce, B. W., De Haan, A. C., Riva, M., Cui, T. Q., Surratt, J. D., Cazaunau, M., Formenti, P., Gratien,
473 A., Pangui, E., and Doussin, J. F.: Methylamine's Effects on Methylglyoxal-Containing Aerosol: Chemical,
474 Physical, and Optical Changes, *Acs Earth and Space Chemistry*, 3, 1706-1716,
475 10.1021/acsearthspacechem.9b00103, 2019.

476 Fu, T. M., Jacob, D. J., Wittrock, F., Burrows, J. P., Vrekoussis, M., and Henze, D. K.: Global budgets of
477 atmospheric glyoxal and methylglyoxal, and implications for formation of secondary organic aerosols, *J.*
478 *Geophys. Res.: Atmos.*, 113, D15303, 10.1029/2007jd009505, 2008.

479 Ge, S., Wang, G., Zhang, S., Li, D., Xie, Y., Wu, C., Yuan, Q., Chen, J., and Zhang, H.: Abundant NH₃ in China
480 enhances atmospheric HONO production by promoting the heterogeneous reaction of SO₂ with NO₂, *Environ.*
481 *Sci. Technol.*, 53, 14339-14347, 10.1021/acs.est.9b04196, 2019.

482 Ge, S. S., Xu, Y. F., and Jia, L.: Effects of inorganic seeds on secondary organic aerosol formation from
483 photochemical oxidation of acetone in a chamber, *Atmos. Environ.*, 170, 205-215,
484 10.1016/j.atmosenv.2017.09.036, 2017.

485 Gen, M., Huang, D. D., and Chan, C. K.: Reactive Uptake of Glyoxal by Ammonium-Containing Salt Particles
486 as a Function of Relative Humidity, *Environ. Sci. Technol.*, 52, 6903-6911, 10.1021/acs.est.8b00606, 2018.

487 Guo, H., Liu, J., Froyd, K. D., Roberts, J. M., Veres, P. R., Hayes, P. L., Jimenez, J. L., Nenes, A., and Weber, R.
488 J.: Fine particle pH and gas–particle phase partitioning of inorganic species in Pasadena, California, during
489 the 2010 CalNex campaign, *Atmos. Chem. Phys.*, 17, 5703–5719, 10.5194/acp-17-5703-2017, 2017.

490 Heald, C. L., Jacob, D. J., Park, R. J., Russell, L. M., Huebert, B. J., Seinfeld, J. H., Liao, H., and Weber, R. J.:
491 A large organic aerosol source in the free troposphere missing from current models, *Geophys. Res. Lett.*, 32,
492 L18809, 10.1029/2005gl023831, 2005.

493 Herrmann, H., Schaefer, T., Tilgner, A., Styler, S. A., Weller, C., Teich, M., and Otto, T.: Tropospheric aqueous-
494 phase chemistry: Kinetics, mechanisms, and its coupling to a changing gas phase, *Chem. Rev.*, 115, 4259-
495 4334, 10.1021/cr500447k, 2015.

496 Huang, D. D., Zhang, X., Dalleska, N. F., Lignell, H., Coggon, M. M., Chan, C. M., Flagan, R. C., Seinfeld, J.
497 H., and Chan, C. K.: A note on the effects of inorganic seed aerosol on the oxidation state of secondary organic
498 aerosol— α -Pinene ozonolysis, *J. Geophys. Res.: Atmos.*, 121, 12476–12483, 10.1002/2016jd025999, 2016.

499 Huang, Y., Zhao, R., Charan, S. M., Kenseth, C. M., Zhang, X., and Seinfeld, J. H.: Unified theory of vapor–
500 wall mass transport in Teflon-walled environmental chambers, *Environ. Sci. Technol.*, 52, 2134–2142,
501 10.1021/acs.est.7b05575, 2018.

502 Jacob, D. J., Field, B. D., Jin, E. M., Bey, I., Li, Q., Logan, J. A., Yantosca, R. M., and Singh, H. B.: Atmospheric
503 budget of acetone, *J. Geophys. Res.: Atmos.*, 107, ACH 5-1–ACH 5-17, 10.1029/2001jd000694, 2002.

504 Jang, M., Czoschke, N. M., Lee, S., and Kamens, R. M.: Heterogeneous Atmospheric Aerosol Production by
505 Acid-Catalyzed Particle-Phase Reactions, *Science*, 298, 814–817, 10.1126/science.1075798, 2002.

506 Ji, Y. M., Shi, Q. J., Li, Y. X., An, T. C., Zheng, J., Peng, J. F., Gao, Y. P., Chen, J. Y., Li, G. Y., Wang, Y., Zhang,
507 F., Zhang, A. L., Zhao, J. Y., Molina, M. J., and Zhang, R. Y.: Carbenium ion-mediated oligomerization of
508 methylglyoxal for secondary organic aerosol formation, *Proc. Natl. Acad. Sci.*, 117, 13294–13299,
509 10.1073/pnas.1912235117, 2020.

510 Jia, L., Xu, Y., and Duan, M.: Explosive formation of secondary organic aerosol due to aerosol-fog interactions,
511 *Sci. Total Environ.*, 866, 161338, 10.1016/j.scitotenv.2022.161338, 2023.

512 Jo, D. S., Nault, B. A., Tilmes, S., Gettelman, A., McCluskey, C. S., Hodzic, A., Henze, D. K., Nawaz, M. O.,
513 Fung, K. M., and Jimenez, J. L.: Global health and climate effects of organic aerosols from different sources,
514 *Environ. Sci. Technol.*, 57, 13793–13807, 10.1021/acs.est.3c02823, 2023.

515 Kampf, C. J., Waxman, E. M., Slowik, J. G., Dommen, J., Pfaffenberger, L., Praplan, A. P., Prévôt, A. S. H.,
516 Baltensperger, U., Hoffmann, T., and Volkamer, R.: Effective Henry’s Law partitioning and the salting constant
517 of glyoxal in aerosols containing sulfate, *Environ. Sci. Technol.*, 47, 4236–4244, 10.1021/es400083d, 2013.

518 Kasthuriarachchi, N. Y., Rivellini, L. H., Chen, X., Li, Y. J., and Lee, A. K. Y.: Effect of relative humidity on
519 secondary brown carbon formation in aqueous droplets, *Environ. Sci. Technol.*, 54, 13207–13216,
520 10.1021/acs.est.0c01239, 2020.

521 Kenseth, C. M., Hafeman, N. J., Rezugui, S. P., Chen, J., Huang, Y., Dalleska, N. F., Kjaergaard, H. G., Stoltz, B.
522 M., Seinfeld, J. H., and Wennberg, P. O.: Particle-phase accretion forms dimer esters in pinene secondary
523 organic aerosol, *Science*, 382, 787–792, 10.1126/science.adi0857, 2023.

524 Li, J., Zhang, H., Li, L., Ye, F., Wang, H., Guo, S., Zhang, N., Qin, M., and Hu, J.: Modeling secondary organic
525 aerosols in China: State of the art and perspectives, *Curr. Pollut. Rep.*, 9, 22–45, 10.1007/s40726-022-00246-
526 3, 2023.

527 Li, Y. X., Zhao, J. Y., Wang, Y., Seinfeld, J. H., and Zhang, R. Y.: Multigeneration production of secondary
528 organic aerosol from toluene photooxidation, *Environ. Sci. Technol.*, 55, 8592–8603, 10.1021/acs.est.1c02026,
529 2021a.

530 Li, Y. X., Ji, Y. M., Zhao, J. Y., Wang, Y., Shi, Q. J., Peng, J. F., Wang, Y. Y., Wang, C. Y., Zhang, F., Wang, Y.

531 X., Seinfeld, J. H., and Zhang, R. Y.: Unexpected oligomerization of small alpha-dicarbonyls for secondary
532 organic aerosol and brown carbon formation, *Environ. Sci. Technol.*, 55, 4430-4439, 10.1021/acs.est.0c08066,
533 2021b.

534 Liu, S., Wang, Y., Xu, X., and Wang, G.: Effects of NO₂ and RH on secondary organic aerosol formation and
535 light absorption from OH oxidation of o-xylene, *Chemosphere*, 308, 136541,
536 10.1016/j.chemosphere.2022.136541, 2022.

537 Liu, S., Huang, D., Wang, Y., Zhang, S., Liu, X., Wu, C., Du, W., and Wang, G.: Synergetic effects of NH₃ and
538 NO_x on the production and optical absorption of secondary organic aerosol formation from toluene
539 photooxidation, *Atmos. Chem. Phys.*, 21, 17759-17773, 10.5194/acp-21-17759-2021, 2021a.

540 Liu, S. J., Wang, Y. Q., Wang, G. H., Zhang, S., Li, D. P., Du, L., Wu, C., Du, W., and Ge, S. S.: Enhancing effect
541 of NO₂ on the formation of light-absorbing secondary organic aerosols from toluene photooxidation, *Sci. Total
542 Environ.*, 794, 148714, 10.1016/j.scitotenv.2021.148714, 2021b.

543 Liu, T. and Abbatt, J. P. D.: Oxidation of sulfur dioxide by nitrogen dioxide accelerated at the interface of
544 deliquesced aerosol particles, *Nat. Chem.*, 13, 1173–1177, 10.1038/s41557-021-00777-0, 2021.

545 Liu, T., Huang, D. D., Li, Z., Liu, Q., Chan, M., and Chan, C. K.: Comparison of secondary organic aerosol
546 formation from toluene on initially wet and dry ammonium sulfate particles at moderate relative humidity,
547 *Atmos. Chem. Phys.*, 18, 5677-5689, 10.5194/acp-18-5677-2018, 2018.

548 Liu, X., Wang, H., Wang, F., Lv, S., Wu, C., Zhao, Y., Zhang, S., Liu, S., Xu, X., Lei, Y., and Wang, G.: Secondary
549 formation of atmospheric brown carbon in China haze: Implication for an enhancing role of ammonia, *Environ.
550 Sci. Technol.*, 57, 11163-11172, 10.1021/acs.est.3c03948, 2023.

551 Liu, Y., Liggio, J., Staebler, R., and Li, S. M.: Reactive uptake of ammonia to secondary organic aerosols: kinetics
552 of organonitrogen formation, *Atmospheric Chemistry and Physics*, 15, 13569-13584, 10.5194/acp-15-13569-
553 2015, 2015.

554 Lv, S., Wu, C., Wang, F., Liu, X., Zhang, S., Chen, Y., Zhang, F., Yang, Y., Wang, H., Huang, C., Fu, Q., Duan,
555 Y., and Wang, G.: Nitrate-enhanced gas-to-particle-phase partitioning of water-soluble organic compounds in
556 Chinese urban atmosphere: Implications for secondary organic aerosol formation, *Environ. Sci. Technol. Lett.*,
557 10, 14-20, 10.1021/acs.estlett.2c00894, 2023.

558 Lv, S., Wang, F., Wu, C., Chen, Y., Liu, S., Zhang, S., Li, D., Du, W., Zhang, F., Wang, H., Huang, C., Fu, Q.,
559 Duan, Y., and Wang, G.: Gas-to-aerosol phase partitioning of atmospheric water-soluble organic compounds
560 at a rural site in China: An enhancing effect of NH₃ on SOA formation, *Environ. Sci. Technol.*, 56, 3915-3924,
561 10.1021/acs.est.1c06855, 2022.

562 Moch, J. M., Dovrou, E., Mickley, L. J., Keutsch, F. N., Liu, Z., Wang, Y., Dombek, T. L., Kuwata, M.,
563 Budisulistiorini, S. H., Yang, L., Decesari, S., Paglione, M., Alexander, B., Shao, J., Munger, J. W., and Jacob,
564 D. J.: Global Importance of Hydroxymethanesulfonate in Ambient Particulate Matter: Implications for Air
565 Quality, *Journal of Geophysical Research: Atmospheres*, 125, D032706, 10.1029/2020jd032706, 2020.

566 Nguyen, T. B., Coggon, M. M., Bates, K. H., Zhang, X., Schwantes, R. H., Schilling, K. A., Loza, C. L., Flagan,
567 R. C., Wennberg, P. O., and Seinfeld, J. H.: Organic aerosol formation from the reactive uptake of isoprene
568 epoxydiols (IEPOX) onto non-acidified inorganic seeds, *Atmos. Chem. Phys.*, 14, 3497-3510, 10.5194/acp-
569 14-3497-2014, 2014.

570 Poulain, L., Katrib, Y., Isikli, E., Liu, Y., Wortham, H., Mirabel, P., Le Calve, S., and Monod, A.: In-cloud
571 multiphase behaviour of acetone in the troposphere: Gas uptake, Henry's law equilibrium and aqueous phase
572 photooxidation, *Chemosphere*, 81, 312-320, 10.1016/j.chemosphere.2010.07.032, 2010.

573 Riva, M., Bell, D. M., Hansen, A.-M. K., Drozd, G. T., Zhang, Z., Gold, A., Imre, D., Surratt, J. D., Glasius, M.,
574 and Zelenyuk, A.: Effect of organic coatings, humidity and aerosol acidity on multiphase chemistry of isoprene

575 epoxydiols, *Environ. Sci. Technol.*, 50, 5580-5588, 10.1021/acs.est.5b06050, 2016.

576 Riva, M., Chen, Y., Zhang, Y., Lei, Z., Olson, N. E., Boyer, H. C., Narayan, S., Yee, L. D., Green, H. S., Cui, T.,
577 Zhang, Z., Baumann, K., Fort, M., Edgerton, E., Budisulistiorini, S. H., Rose, C. A., Ribeiro, I. O., e Oliveira,
578 R. L., dos Santos, E. O., Machado, C. M. D., Szopa, S., Zhao, Y., Alves, E. G., de Sá, S. S., Hu, W., Knipping,
579 E. M., Shaw, S. L., Duvoisin Junior, S., de Souza, R. A. F., Palm, B. B., Jimenez, J.-L., Glasius, M., Goldstein,
580 A. H., Pye, H. O. T., Gold, A., Turpin, B. J., Vizuete, W., Martin, S. T., Thornton, J. A., Dutcher, C. S., Ault,
581 A. P., and Surratt, J. D.: Increasing isoprene epoxydiol-to-inorganic sulfate aerosol ratio results in extensive
582 conversion of inorganic sulfate to organosulfur forms: Implications for aerosol physicochemical properties,
583 *Environ. Sci. Technol.*, 53, 8682-8694, 10.1021/acs.est.9b01019, 2019.

584 Rodriguez, A. A., de Loera, A., Powelson, M. H., Galloway, M. M., and Haan, D. O.: Formaldehyde and
585 Acetaldehyde Increase Aqueous-Phase Production of Imidazoles in Methylglyoxal/Amine Mixtures:
586 Quantifying a Secondary Organic Aerosol Formation Mechanism, *Environmental Science & Technology*
587 *Letters*, 4, 234-239, 10.1021/acs.estlett.7b00129, 2017.

588 Seinfeld, J. H. and Pandis, S. N.: *ATMOSPHERIC CHEMISTRY AND PHYSICS: from air pollution to climate*
589 *change*, John Wiley & Sons 2006.

590 Shen, C., Zhang, W., Choczynski, J., Davies, J. F., and Zhang, H.: Phase state and relative humidity regulate the
591 heterogeneous oxidation kinetics and pathways of organic-inorganic mixed aerosols, *Environ. Sci. Technol.*,
592 56, 15398-15407, 10.1021/acs.est.2c04670, 2022.

593 Srivastava, D., Vu, T. V., Tong, S., Shi, Z., and Harrison, R. M.: Formation of secondary organic aerosols from
594 anthropogenic precursors in laboratory studies, *npj Clim. Atmos. Sci.*, 5, 22, 10.1038/s41612-022-00238-6,
595 2022.

596 Wang, C., Lei, Y. D., and Wania, F.: Effect of sodium sulfate, ammonium chloride, ammonium nitrate, and salt
597 mixtures on aqueous phase partitioning of organic compounds, *Environ. Sci. Technol.*, 50, 12742-12749,
598 10.1021/acs.est.6b03525, 2016a.

599 Wang, F., Lv, S., Liu, X., Lei, Y., Wu, C., Chen, Y., Zhang, F., and Wang, G.: Investigation into the differences
600 and relationships between gasSOA and aqSOA in winter haze pollution on Chongming Island, Shanghai, based
601 on VOCs observation, *Environ. Pollut.*, 316, 120684, 10.1016/j.envpol.2022.120684, 2023.

602 Wang, G., Zhang, R., Gomez, M. E., Yang, L., Levy Zamora, M., Hu, M., Lin, Y., Peng, J., Guo, S., Meng, J., Li,
603 J., Cheng, C., Hu, T., Ren, Y., Wang, Y., Gao, J., Cao, J., An, Z., Zhou, W., Li, G., Wang, J., Tian, P., Marrero-
604 Ortiz, W., Secretst, J., Du, Z., Zheng, J., Shang, D., Zeng, L., Shao, M., Wang, W., Huang, Y., Wang, Y., Zhu,
605 Y., Li, Y., Hu, J., Pan, B., Cai, L., Cheng, Y., Ji, Y., Zhang, F., Rosenfeld, D., Liss, P. S., Duce, R. A., Kolb, C.
606 E., and Molina, M. J.: Persistent sulfate formation from London Fog to Chinese haze, *Proc. Natl. Acad. Sci.*,
607 113, 13630-13635, 10.1073/pnas.1616540113, 2016b.

608 Wang, Y., Cui, S., Fu, X., Zhang, Y., Wang, J., Fu, P., Ge, X., Li, H., and Wang, X.: Secondary organic aerosol
609 formation from photooxidation of C₃H₆ under the presence of NH₃: Effects of seed particles, *Environ. Res.*,
610 211, 113064, 10.1016/j.envres.2022.113064, 2022.

611 Waxman, E. M., Elm, J., Kurtén, T., Mikkelsen, K. V., Ziemann, P. J., and Volkamer, R.: Glyoxal and
612 methylglyoxal setschenow salting constants in sulfate, nitrate, and chloride solutions: Measurements and gibbs
613 energies, *Environ. Sci. Technol.*, 49, 11500-11508, 10.1021/acs.est.5b02782, 2015.

614 Wei, J., Fang, T., and Shiraiwa, M.: Effects of acidity on reactive oxygen species formation from secondary
615 organic aerosols, *ACS Environ. Au*, 2, 336-345, 10.1021/acsenvironau.2c00018, 2022.

616 Wong, J. P. S., Lee, A. K. Y., and Abbatt, J. P. D.: Impacts of sulfate seed acidity and water content on isoprene
617 secondary organic aerosol formation, *Environ. Sci. Technol.*, 49, 13215-13221, 10.1021/acs.est.5b02686,
618 2015.

619 Yang, L., Huang, R.-J., Yuan, W., Huang, D. D., and Huang, C.: pH-dependent aqueous-phase brown carbon
620 formation: Rate constants and implications for solar absorption and atmospheric photochemistry, *Environ. Sci.*
621 *Technol.*, 58, 1236-1243, 10.1021/acs.est.3c07631, 2024.

622 Yaremko, I. A., Vil', V. A., Demchuk, D. V., and Terent'ev, A. O.: Rearrangements of organic peroxides and
623 related processes, *Beilstein J. Org. Chem.*, 12, 1647-1748, 10.3762/bjoc.12.162, 2016.

624 Yasmeen, F., Sauret, N., Gal, J. F., Maria, P. C., Massi, L., Maenhaut, W., and Claeys, M.: Characterization of
625 oligomers from methylglyoxal under dark conditions: a pathway to produce secondary organic aerosol through
626 cloud processing during nighttime, *Atmospheric Chemistry and Physics*, 10, 3803-3812, 10.5194/acp-10-
627 3803-2010, 2010.

628 You, B., Li, S. Y., Tsona, N. T., Li, J. L., Xu, L., Yang, Z. M., Cheng, S. M., Chen, Q. C., George, C., Ge, M. F.,
629 and Du, L.: Environmental processing of short-chain fatty alcohols induced by photosensitized chemistry of
630 brown carbons, *ACS Earth Space Chem.*, 4, 631-640, 10.1021/acsearthspacechem.0c00023, 2020.

631 Zhang, J., Shrivastava, M., Zelenyuk, A., Zaveri, R. A., Surratt, J. D., Riva, M., Bell, D., and Glasius, M.:
632 Observationally constrained modeling of the reactive uptake of isoprene-derived epoxydiols under elevated
633 relative humidity and varying acidity of seed aerosol conditions, *ACS Earth Space Chem.*, 7, 788-799,
634 10.1021/acsearthspacechem.2c00358, 2023.

635 Zhang, R., Wang, G., Guo, S., Zamora, M. L., Ying, Q., Lin, Y., Wang, W., Hu, M., and Wang, Y.: Formation of
636 urban fine particulate matter, *Chem. Rev.*, 115, 3803-3855, 10.1021/acs.chemrev.5b00067, 2015a.

637 Zhang, S., Li, D., Ge, S., Wu, C., Xu, X., Liu, X., Li, R., Zhang, F., and Wang, G.: Elucidating the mechanism
638 on the transition-metal ion-synergetic-catalyzed oxidation of SO₂ with implications for sulfate formation in
639 Beijing haze, *Environ. Sci. Technol.*, 58, 2912-2921, 10.1021/acs.est.3c08411, 2024.

640 Zhang, S., Li, D., Ge, S., Liu, S., Wu, C., Wang, Y., Chen, Y., Lv, S., Wang, F., Meng, J., and Wang, G.: Rapid
641 sulfate formation from synergetic oxidation of SO₂ by O₃ and NO₂ under ammonia-rich conditions:
642 Implications for the explosive growth of atmospheric PM_{2.5} during haze events in China, *Sci. Total Environ.*,
643 772, 144897, 10.1016/j.scitotenv.2020.144897, 2021.

644 Zhang, X., Schwantes, R. H., McVay, R. C., Lignell, H., Coggon, M. M., Flagan, R. C., and Seinfeld, J. H.: Vapor
645 wall deposition in Teflon chambers, *Atmos. Chem. Phys.*, 15, 4197-4214, 10.5194/acp-15-4197-2015, 2015b.

646 Zhang, Y. M., He, L., Sun, X. M., Ventura, O. N., and Herrmann, H.: Theoretical Investigation on the
647 Oligomerization of Methylglyoxal and Glyoxal in Aqueous Atmospheric Aerosol Particles, *Acs Earth and*
648 *Space Chemistry*, 6, 1031-1043, 10.1021/acsearthspacechem.1c00422, 2022.

649 Zhao, J., Levitt, N. P., Zhang, R., and Chen, J.: Heterogeneous Reactions of methylglyoxal in acidic media:
650 Implications for secondary organic aerosol formation, *Environ. Sci. Technol.*, 40, 7682-7687,
651 10.1021/es060610k, 2006.

652 Zhao, R., Aljawhary, D., Lee, A. K. Y., and Abbatt, J. P. D.: Rapid aqueous-phase photooxidation of dimers in
653 the α -pinene secondary organic aerosol, *Environ. Sci. Technol. Lett.*, 4, 205-210, 10.1021/acs.estlett.7b00148,
654 2017.

655

656

657

658

659

660

661

662

663 **Table 1.** Concentrations of total SOA formed in the chamber and that formed only from the
 664 uptake of methylglyoxal (MGly) in the chamber

Seed	SOA ^a ($\mu\text{g m}^{-3}$)	Surface area of seeds ($\text{m}^2 \text{m}^{-3}$)	MGly ($\mu\text{g m}^{-3}$)	γ^b	SOA _{MGly} ^c ($\mu\text{g m}^{-3}$)	SOA/SOA _{MGly}
Na ₂ SO ₄	140	9.30×10^{-3}	26.74	2.6×10^{-4}	17.17	8.2
(NH ₄) ₂ SO ₄	101	1.95×10^{-2}	42.95	2.6×10^{-4}	28.88	3.5
NH ₄ HSO ₄	57	1.14×10^{-2}	38.43	2.6×10^{-4}	20.17	2.8

665 ^aSOA values are the concentrations of SOA on different seeds observed in the experiments. ^bThe values of
 666 γ are consistent with the parameters of the irreversible uptake of MGly used in CMAQ v5.3. ^cSOA_{MGly} is
 667 estimated concentration of SOA formed from the irreversible uptake of MGly on different aerosols.
 668

669

670

671

672

673

674

Figure Captions

675 **Figure 1.** Time evolution of gas-phase and aerosol-phase species in the presence of
676 $(\text{NH}_4)_2\text{SO}_4$ seeds during acetone oxidation process (Phase I: Photochemical reactions of
677 acetone by OH radicals without NH_3 ; Phase II: Reaction of acetone oxidation products with
678 NH_3 under dark conditions) (a) Gas-phase compounds; (b) SOA and molar ratio of NH_4^+ to
679 SO_4^{2-} in the aerosol-phase; (c) N/C and O/C elemental ratios and oxidation state of
680 compounds (OSc, $2 \times \text{O}/\text{C}-\text{H}/\text{C}$) of SOA; (d) Relative abundances of CO_2^+ , the sum of CHO^+
681 plus $\text{C}_2\text{H}_3\text{O}^+$, and CHN family fragments of SOA.

682

683

684

685 **Figure 2.** Fragment compositions of acetone-derived SOA in the presence of $(\text{NH}_4)_2\text{SO}_4$
686 seeds between the two reaction phases. (Phase I: Oxidation of acetone by OH radicals
687 without NH_3 ; Phase II: Reaction of acetone oxidation products with NH_3 under dark
688 conditions)

689

690

691 **Figure 3.** Effect of seed acidity on SOA formation. (a) The amount SOA normalized by the
692 surface area (SA) of aerosols and OSc of SOA in the presence of different seeds at Phase I;
693 (b) Effective Henry's law constants ($K_{\text{H, salt}}$) of MGly and acidity (pH) of inorganic aerosols
694 during the reaction; (c) and (d) Mass spectra of SOA from acetone oxidations by OH
695 radicals with no NH_3 in the presence of Na_2SO_4 and $(\text{NH}_4)_2\text{SO}_4$ seeds, respectively.

696

697

698 **Figure 4.** Effect of ammonia on SOA formation. (a) The Difference in N/C ratio of Phase II
699 relative to Phase I on different seeds; (b) Partitioning coefficients of NH_3 ($\epsilon(\text{NH}_4^+)$) on
700 different seeds in the chamber; (c) MAC of acetone-derived SOA in the presence of different
701 seeds; (d) Mass spectrum of 1H-imidazole-4-carboxylic acid formed during the
702 heterogeneous oxidation of acetone in the presence of $(\text{NH}_4)_2\text{SO}_4$ seed.

703

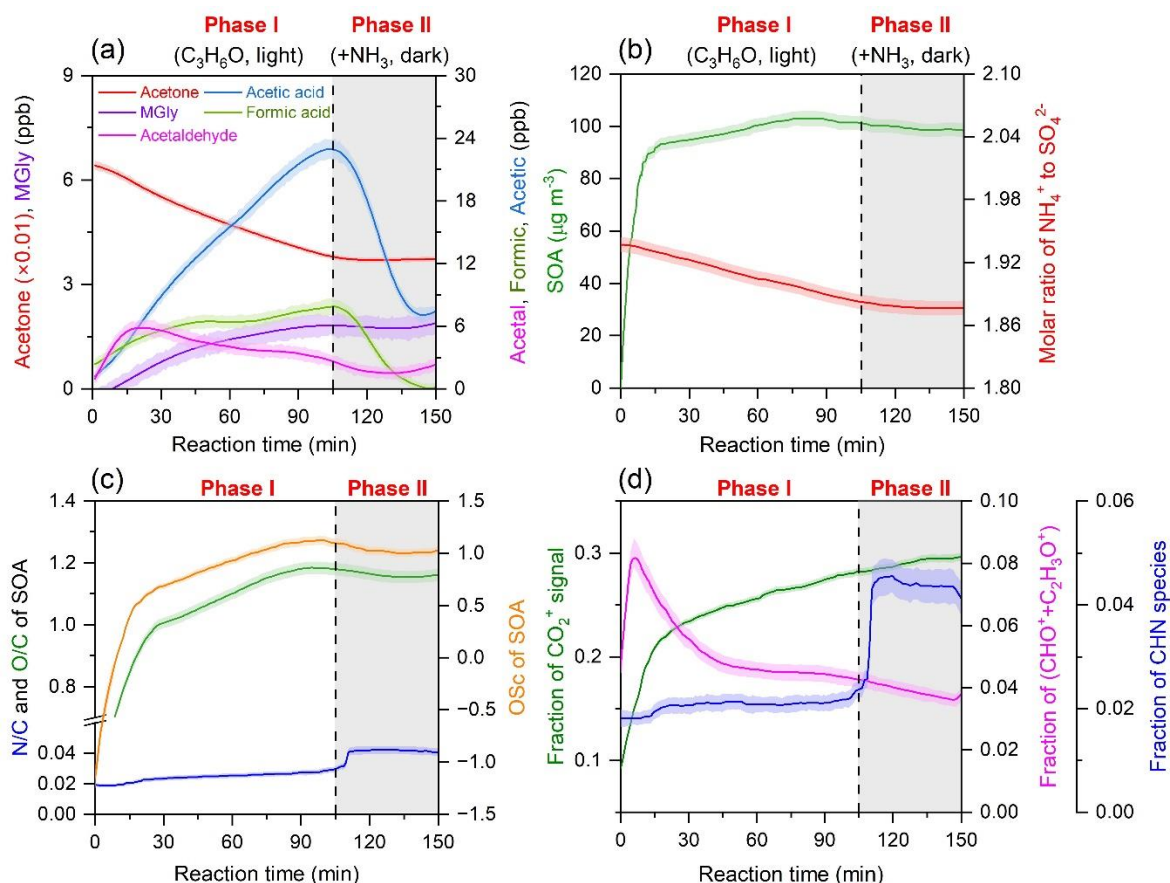
704

705 **Figure 5.** SOA yield (green) and $\text{MAC}_{\lambda=270 \text{ nm}}$ (red) of acetone-derived SOA in the presence
706 of Na_2SO_4 and $(\text{NH}_4)_2\text{SO}_4$ seeds with NH_3 under dark conditions (Phase II), respectively.

707

708 **Figure 6.** A diagram for the formation pathway of SOA derived from acetone oxidation in
709 the atmosphere.

710



711

712 **Figure 1.** Time evolution of gas-phase and aerosol-phase species in the presence of
 713 $(NH_4)_2SO_4$ seeds during acetone oxidation process (Phase I: Photochemical reactions of
 714 acetone by OH radicals without NH_3 ; Phase II: Reaction of acetone oxidation products with
 715 NH_3 under dark conditions) (a) Gas-phase compounds; (b) SOA and molar ratio of NH_4^+ to
 716 SO_4^{2-} in the aerosol-phase; (c) N/C and O/C elemental ratios and oxidation state of
 717 compounds (OSc, $2 \times O/C - H/C$) of SOA; (d) Relative abundances of CO_2^+ , the sum of CHO^+
 718 plus $C_2H_3O^+$, and CHN family fragments of SOA.

719

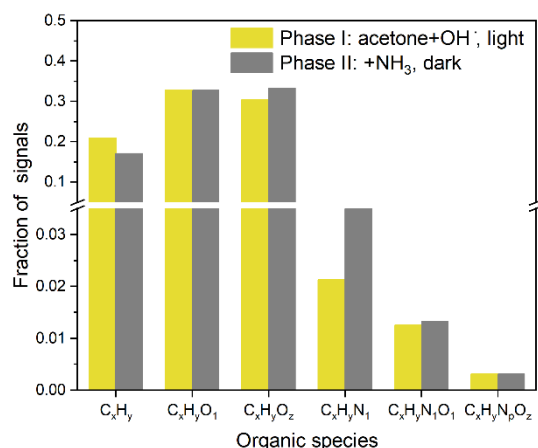
720

721

722

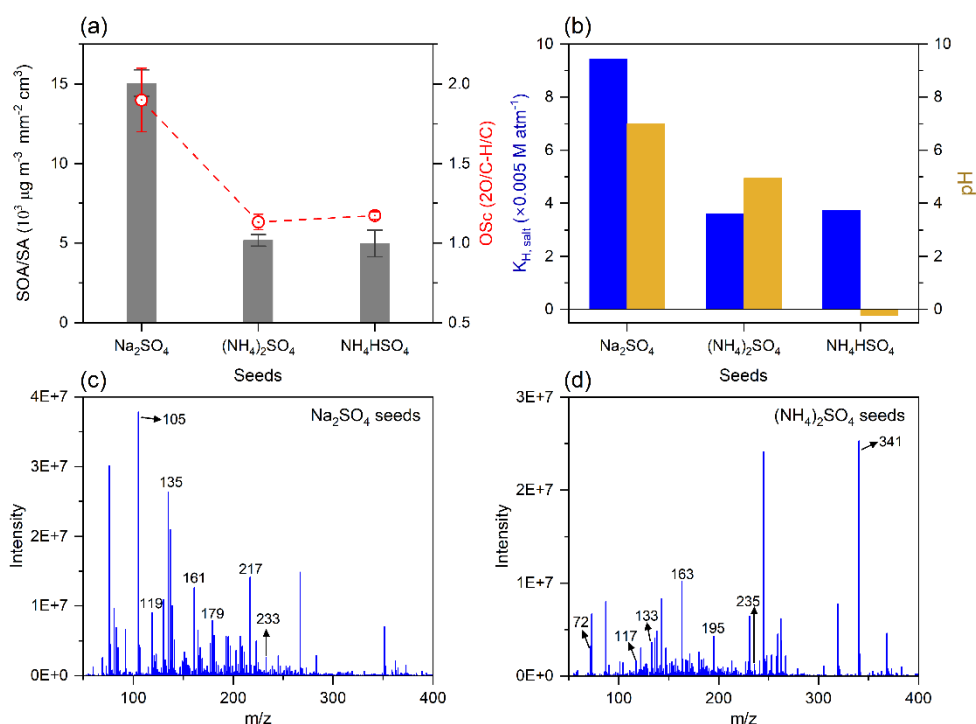
723

724



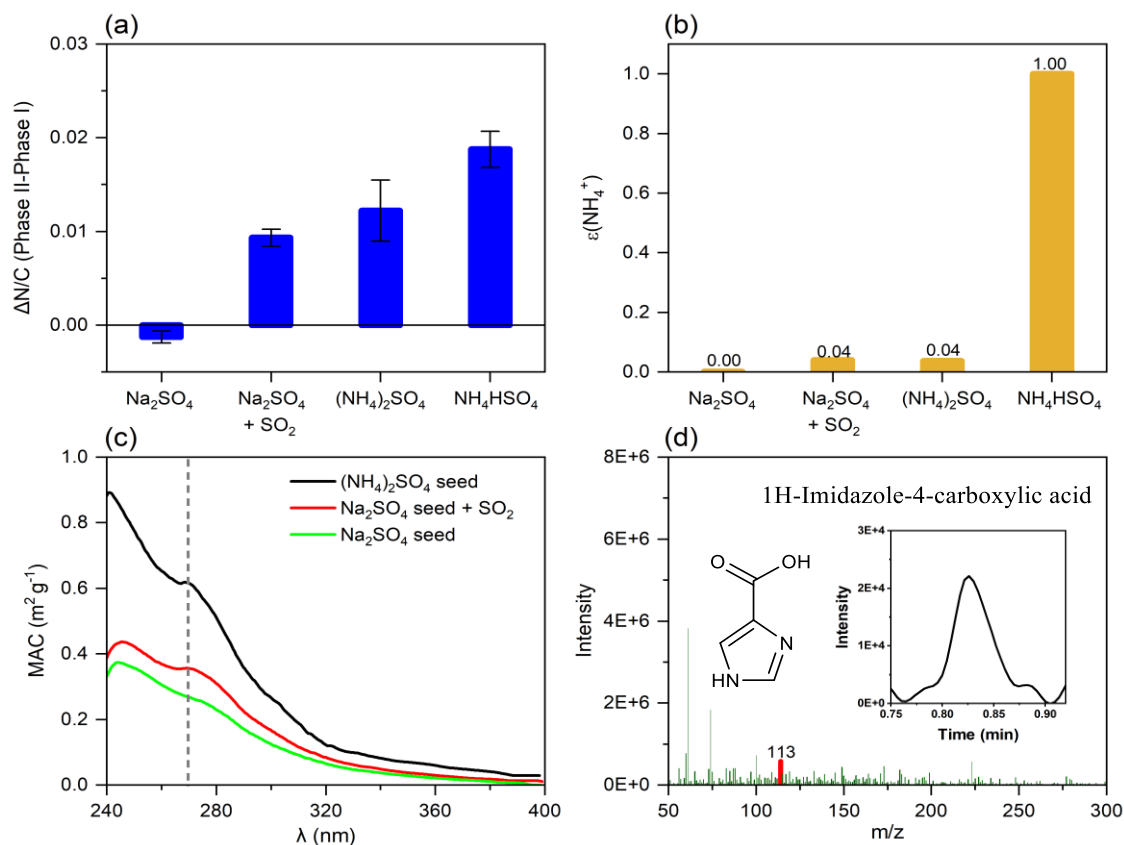
725
726
727
728
729
730
731
732

Figure 2. Fragment compositions of acetone-derived SOA in the presence of (NH₄)₂SO₄ seeds between the two reaction phases. (Phase I: Oxidation of acetone by OH radicals without NH₃; Phase II: Reaction of acetone oxidation products with NH₃ under dark conditions)



733
734
735
736
737
738

Figure 3. Effect of seed acidity on SOA formation. (a) The amount SOA normalized by the surface area (SA) of aerosols and OSc of SOA in the presence of different seeds at Phase I; (b) Effective Henry's law constants ($K_{\text{H, salt}}$) of MGly and acidity (pH) of inorganic aerosols during the reaction; (c) and (d) Mass spectra of SOA from acetone oxidations by OH radicals with no NH₃ in the presence of Na₂SO₄ and (NH₄)₂SO₄ seeds, respectively.



739

740 **Figure 4.** Effect of ammonia on SOA formation. (a) The Difference in N/C ratio of Phase II
 741 relative to Phase I on different seeds; (b) Partitioning coefficients of NH₃ ($\epsilon(\text{NH}_4^+)$) on
 742 different seeds in the chamber; (c) MAC of acetone-derived SOA in the presence of different
 743 seeds; (d) Mass spectrum of 1H-imidazole-4-carboxylic acid formed during the
 744 heterogeneous oxidation of acetone in the presence of (NH₄)₂SO₄ seed.

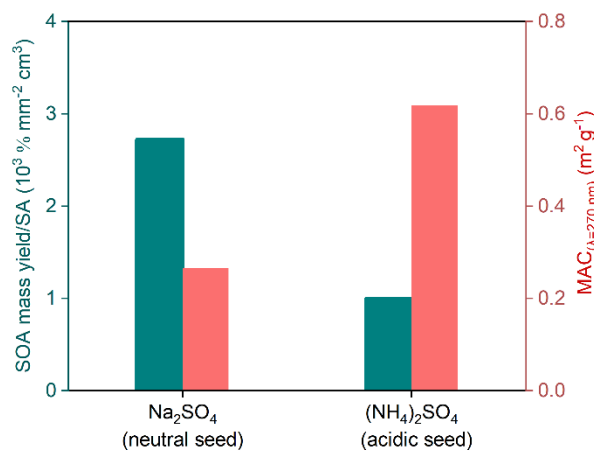
745

746

747

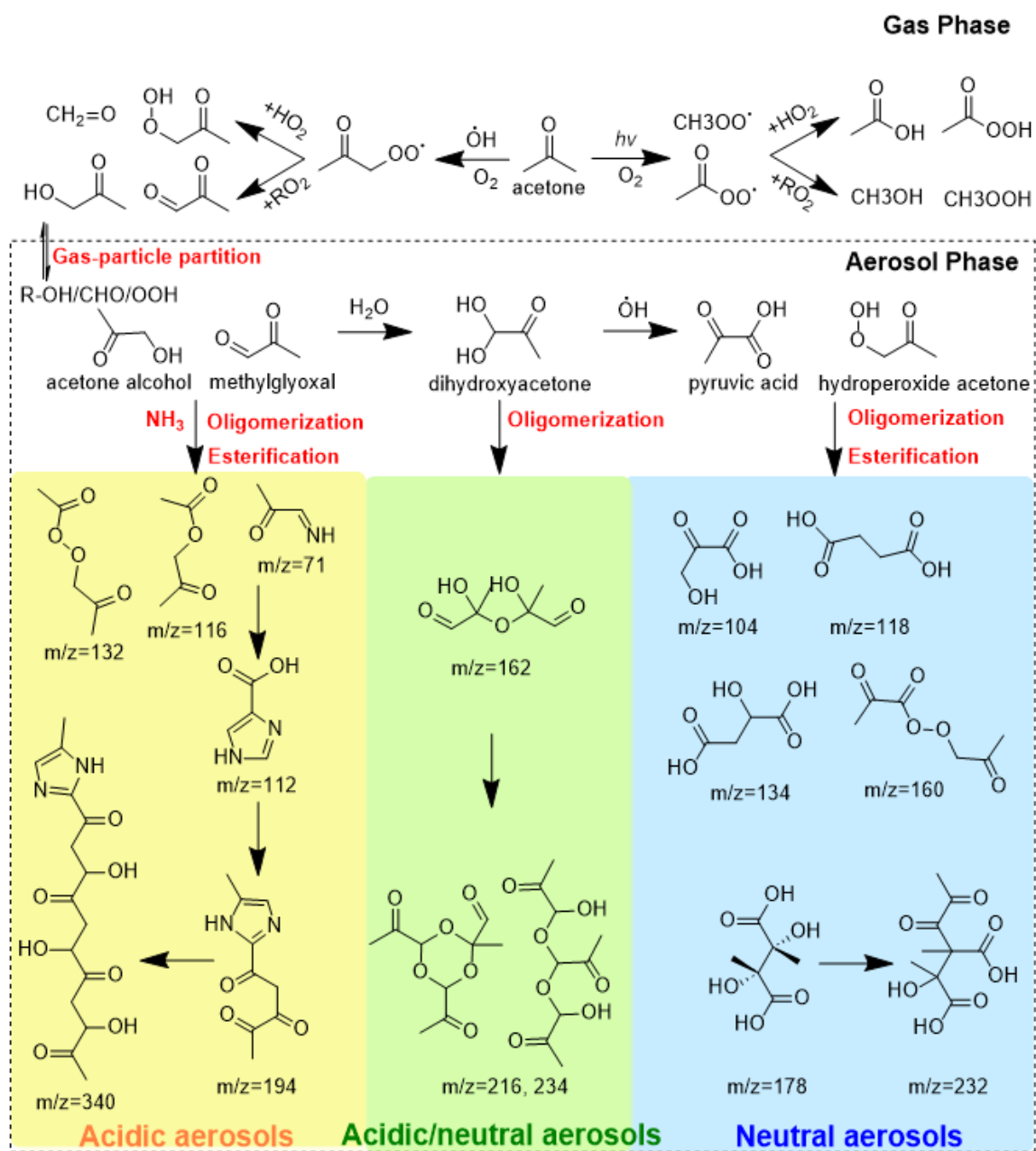
748

749



750

751 **Figure 5.** SOA yield (green) and MAC_{λ=270 nm} (red) of acetone-derived SOA in the presence
 752 of Na₂SO₄ and (NH₄)₂SO₄ seeds with NH₃ under dark conditions (Phase II), respectively.



754

755 **Figure 6.** A diagram for the formation pathway of SOA derived from acetone oxidation in
 756 the atmosphere.

757